Numerical investigation of the rheological behavior of a dense particle suspension in a biviscous matrix using a lubrication dynamics method

S.S. Prasanna Kumar,[1, a)] A. Vázquez-Quesada,[2] and M. Ellero[1, 3, 4]

[1)] *Basque Center for Applied Mathematics (BCAM), Alameda de Mazarredo 14, 48400 Bilbao, Spain*

[2)] *Department of Theoretical Condensed Matter Physics, Universidad Autónoma de Madrid, Madrid, Spain*

[3)] *IKERBASQUE, Basque Foundation for Science, Calle de María Díaz de Haro 3, 48013 Bilbao, Spain*

[4)] *Zienkiewicz Centre for Computational Engineering (ZCCE), Swansea University, Bay Campus, Swansea SA1 8EN, United Kingdom*

(Dated:; Revised)

This paper presents a numerical approach to predict the rheology of dense non-colloidal suspensions with a biviscous matrix. A biviscous matrix is characterized as a fluid with two shear rate dependent viscosities i.e. one above and below a critical shear rate $\dot{\gamma}_c$. The methodology is based on the lubrication dynamics which dominantly influence the suspension properties at high values of particle concentration. To efficiently handle the singular lubrication forces in the dense suspensions, a semi-implicit splitting integration scheme is employed. Using the presented approach, three dimensional simulations were performed and the predicted rheology of the suspension with a biviscous matrix is discussed under two regimes: (a) $\dot{\gamma}_c$ larger than the macroscopic applied shear rate where fluid slippage effect can be modeled in terms of the non-Newtonian properties of the matrix, and (2) $\dot{\gamma}_c$ smaller than the macroscopic applied shear rate where a biviscous model can be seen as a regularization of an apparent yield stress matrix. The results obtained at high $\dot{\gamma}_c$ show that the shear thinning of the biviscous matrix in the inter-particle gaps, which can be interpreted as an apparent fluid slipping on the particle surface, provides an alternative mechanism to explain the experimentally observed shear-thinning of non-colloidal suspension with Newtonian matrices. At low $\dot{\gamma}_c$ values, the predicted suspension properties and its microstructure corroborates the available experimental results on suspensions with yield stress fluids.

[a)]Electronic mail: ssavarimuthu@bcamath.org

I. INTRODUCTION

The non-linear rheological properties of non-colloidal suspensions are intrinsically originating from the complex particle-fluid interactions which, in the case of non-Newtonian solvent matrices, is the subject of intense research [1–8]. Tunable properties of such fluids hold tremendous industrial impact and thereby offers a challenging problem of understanding their flow behavior under different conditions. For example, flow of complex suspensions involving fine-grained sediments (e.g. clays, silt or sand) often arise in coastal and offshore engineering applications and therefore novel particle-level models are crucial to predict sediment's rheology and transport accurately. Although there are many factors that contribute to make the rheological response of suspensions complex (e.g. interparticle interaction, particle shape etc.), even the "simple" case of hard spheres suspended in a Newtonian matrix can present significant complications when the volume fraction of the suspended phase is sufficiently increased. In the case of dense systems, beside the increasing importance of non-hydrodynamic contact forces [9, 10], the dominance of the near-contact singular lubrication forces between the particles at close separation is one of the many factors that pose modeling and numerical challenges.

Characterization of a given suspension is conventionally carried-out in experiments using a rheometer to measure the standard rheometric functions such as the suspension viscosity. A complementary approach is to numerically simulate simple rheology tests using appropriate mathematical models. Fully-resolved Direct Numerical Simulation (DNS) of the particle suspensions using conventional mesh-based methods [1, 11–14] and meshless methods [15–17] already exist. However, these techniques require higher computational resources to resolve the very small inter-particle separation under near contact conditions which frequently arise in dense systems at large particle volume fraction and/or applied shear rates. The requirement for such methodologies to resolve very thin regions of space often restricts the number of particles employed to a few hundreds and/or the physical dimensions to two. Alternatively, methods such as Accelerated Stokesian Dynamics [18], Fast Stokesian Dynamics [19], Dissipative Particle Dynamics [20], Lattice-Boltzmann method [21] have incorporated the effect of short-range hydrodynamic interactions analytically. In the Smoothed Particle Hydrodynamics method presented in [22], the flow around single particles is fully resolved, whereas the

flow in the gap between two particles is resolved up to a given threshold distance. At smaller gaps analytical solutions for the interstitial flow between particle pairs is used, thus effectively overcoming the need for higher/adaptive spatial resolution. With further improvement on the numerical techniques aiming at the optimization of time stepping, such as the semi-implicit splitting integration scheme [23, 24], simulating systems with thousands of particles in three dimensions for large time scales is already realizable.

Beside the requirement of high computational resources to simulate dense particulate systems, another serious limitation of the aforementioned methods is the additional modeling difficulties that may arise when considering non-Newtonian suspending media. Irrespective of the solver being used, either an implicit or an explicit type, it is somewhat difficult with the current methodologies to simulate three-dimensional complex fluid flow problems even with few thousands of particles. Even for a simple flow such as a Couette flow, the popular Stokesian Dynamics solver and its variants resort to careful reduction of the computational cost by approximating the full many-body far-field hydrodynamic interactions by means of particle-drag self-terms and considering only the short-range lubrication interactions. Such methods that expedite the calculations are now known as Fast Lubrication Dynamics (FLD) [25, 26]. Despite the obvious advantage, such simplifications might lead to artifacts when particles are exposed to external forcing or when flow details (e.g., diffusion or velocity correlations) are needed, and therefore caution should be exercised in setting the simulation parameters [27]. While the accuracy and performance owing to such simplification has been reported in the case of implicit methods such as Stokesian Dynamics, none has been reported when explicit integration of the lubrication equations are carried-out.

Numerical estimation of the rheological properties and micro-structure of a variety of non-colloidal suspensions have been reported in the literature. Apart from the size, shape, dispersity, rigidity and volume fraction of the suspended particles, the influence of the shear rate dependent viscosity of the suspending medium on the rheology of the suspension is also of particular importance. To this end, the rheology of non-colloidal hard spheres suspended in *continuous* shear thickening and shear thinning matrices has been studied [2, 3, 5, 6, 28]. However, to the best of our knowledge, numerical studies on suspensions with solvent that has *discontinuous* variation of its viscosity with shear rate is still lacking. Moreover, in the case of dense particle systems with highly non-Newtonian suspending media the critical challenge is

represented by the choice of the interparticle lubrication force model (rather than the far-field contributions which are generally screened) which cannot always be accurately approximated by Newtonian-like expressions [29] with modified non-Newtonian viscosity [2, 3, 28].

A simple approach to model a discontinuous shear rate dependency of matrices is through the *biviscous* model. This model was originally proposed by Tanner and Milthorpe [30] as an alternative to the other popular models such as the Bingham model, Herschel-Bulkley model or Casson model [31] to simulate the *apparent yield stress* fluids. It employs two viscosities, a relatively larger η_0 for $\dot{\gamma} \leq \dot{\gamma}_c$ and a small η_1 for $\dot{\gamma} > \dot{\gamma}_c$. In the case of fluid matrices characterized by a true yield stress σ^y, the biviscous model allows, for a given plastic viscosity η_0, to calculate a sufficiently small value for the $\dot{\gamma}$ to regularize the transition and mimic an apparent yielding behavior. Although this approach is similar to the other regularization approaches, such as the widely employed exponential regularization of Papanastasiou [32], it provides further mathematical and computational simplicity and has allowed to derive the corresponding solution for the interparticle lubrication analytically [33]. The biviscous model has been successfully employed in the the works of Tanner and Milthorpe [30], Beverly and Tanner [34] and Prashant and Derksen [35]. In the case the fluid matrix is defined by an apparent yield stress - and the true low-shear rate viscous behaviour can be experimentally characterized - the present biviscous model is able to parametrize the large zero-shear-rate viscosity plateau and its corresponding transition in the shear rate [36]. In both cases, the rheology of a dense non-colloidal suspension with a biviscous matrix has not been studied yet.

It should be remarked that another interesting utility of the biviscous model lies in its ability to model also *apparent slippage effects* by setting a large value for the critical shear rate $\dot{\gamma}_c$ and taking the low shear rate viscosity η_0 being equal to the bulk value. In a recent study, Kroupa et al. [37] established a connection between the decrease in the viscosity of a concentrated non-colloidal suspension with shear rate and the slipping of the solvent on the particle surface. As the effect of slip between the particles and the solvent can be expected to grow with particle volume fraction and applied shear, it is likely to extend a dominating influence on the rheology of the concentrated suspensions. In another study, Vázquez-Quesada et al. [38] showed that the apparent slipping of the matrix fluid in the interstitial gap between a particle pair can be modeled directly by using the lubrication force

expressions for a biviscous fluid, i.e through the shear-rate dependent thinning of the matrix. With the critical shear rate $\dot{\gamma}_c$ and the viscosity ratio η_1/η_0 of the biviscous model as the relevant calibration parameters, effective interparticle lubrication interactions were presented that compared well with those inferred by the experiments and from slip theories [38]. These findings further strengthen the existence of hidden shear rate effects, such as the apparent slippage, as a possible explanation on the physical mechanisms behind the shear thinning of non-colloidal hard-sphere suspensions when Newtonian solvents are used [5]. On opposite, in the case of weakly non-Newtonian low molecular weight silicon oils the real thinning of the matrix, even occurring at very large shear rates, can also deliver the shear-thinning of the suspension [28]. It is therefore compelling to numerically characterize the rheological behavior of a non-colloidal suspension with a biviscous matrix model.

In this paper, we aim to numerically study the rheology of non-colloidal particles suspended in a biviscous matrix. Employing several thousands of particles, three dimensional simulations are performed to study the rheology of *dense* suspensions in two limits: (1) for $\dot{\gamma}_c$ larger than the macroscopic applied shear rate, i.e. where the fluid apparent slip effect is recovered; and (2) $\dot{\gamma}_c$ smaller the macroscopic applied shear rate where a biviscous model can be seen as a regularization of an apparent yield stress matrix. To this end, we present in Section II the numerical methodology employed in the present study. Section III begins with validation of the employed models, followed by the discussion on the rheology of a dense non-colloidal suspensions with biviscous matrix. The discussions are split into two parts: Section III B 1 presents the effect of interparticle apparent fluid slippage on the suspension rheology modeled by high critical shear rate, whereas Section III B 2 presents the rheology of a suspension with an apparent yield stress matrix modeled by a very low critical shear rate in the biviscosity model. The paper concludes with a brief summary in Section IV.

II. SOLUTION METHODOLOGY

In this section the details of the suspension model are presented along with the numerical techniques employed for carrying out the simulations.

A. Modeling dense non-colloidal suspension with a Newtonian matrix

By neglecting the contribution of contact frictional forces (e.g. in some surfactants/polymers-stabilized particulate systems with extremely low coefficients of friction [39]) at higher values of particle volume fraction ϕ (defined as the ratio of particle volume to total volume), the rheology of a given suspension is dominantly influenced by the singular short-range lubrication force between pairs of suspended particles. These forces arise from the relative motion of the particles at very close separation that are classified into different modes. The lubrication force under the squeeze ($\mathbf{F}^n$) and shear ($\mathbf{F}^t$) modes acting between pairs of particles (say α and β) are as follows:

$$\mathbf{F}^n_{\alpha\beta} = f_{\alpha\beta}(h)\mathbf{V}_{\alpha\beta} \cdot \mathbf{e}_{\alpha\beta}\mathbf{e}_{\alpha\beta} \tag{1}$$

$$\mathbf{F}^t_{\alpha\beta} = g_{\alpha\beta}(h)\mathbf{V}_{\alpha\beta} \cdot (\mathbf{1}-\mathbf{e}_{\alpha\beta}\mathbf{e}_{\alpha\beta}) \tag{2}$$

where,

$$f_{\alpha\beta}(h) = -6\pi\eta \left[\left(\frac{a_\alpha a_\beta}{a_\alpha + a_\beta} \right)^2 \frac{1}{h} + a_\alpha \left(\frac{1 + 7\frac{a_\beta}{a_\alpha} + \left(\frac{a_\beta}{a_\alpha}\right)^2}{5\left(1+\frac{a_\beta}{a_\alpha}\right)^3} \right) ln\left(\frac{a_\alpha}{h}\right) \right] \quad \text{and} \tag{3}$$

$$g_{\alpha\beta}(h) = -6\pi\eta a_\alpha \left[\frac{4\frac{a_\beta}{a_\alpha}\left(2 + \frac{a_\beta}{a_\alpha} + 2\left(\frac{a_\beta}{a_\alpha}\right)^2\right)}{15\left(1+\frac{a_\beta}{a_\alpha}\right)^3} ln\left(\frac{a_\alpha}{h}\right) \right]. \tag{4}$$

Here, $\mathbf{V}_{\alpha\beta}$ is the relative velocity of a particle pair and $f_{\alpha\beta}$ and $g_{\alpha\beta}$ are scalar functions which depends on the size (a is the radius of a particle), inter-particle gap (h) and dynamic viscosity of the matrix fluid (η). For simulating dense suspensions, i.e. with value of $\phi \geq 0.4$, the long-range hydrodynamic forces can be generally ignored, as they are much smaller than the singular lubrication forces, to enable simpler and faster methods to study their rheological properties. As a mean for further simplification, earlier studies [40, 41] have considered only the lubrication force corresponding to the squeeze mode. Although less accurate when used in absence of an explicit numerical treatment of the solvent, such models are adequate to qualitatively demonstrate the peculiar rheological behavior of dense non-colloidal suspensions. In particular, this work focuses on a modification of the normal lubrication force under squeeze mode alone for a viscoplastic matrix modeled as a biviscous fluid and aims at the study of its effect on the suspension rheology in comparison to the classical Newtonian lubrication model.

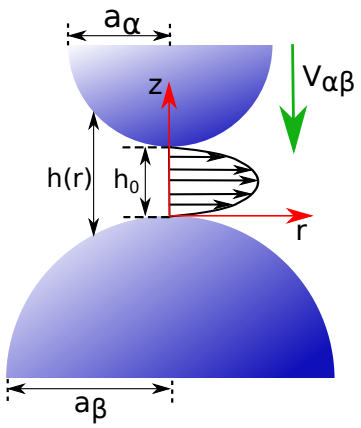

FIG. 1: Schematic of two spheres interacting in a squeeze mode.

B. Modeling dense non-colloidal suspension with a biviscous matrix

In the present work, a non-colloidal suspension with a biviscous shear thinning matrix is studied. The sudden drop in dynamic viscosity at a specific value of shear rate for a shear thinning fluid can be formulated as,

$$\eta = \begin{cases} \eta_0, & \text{if } |\dot{\gamma}| < \dot{\gamma}_c, \\ \eta_1, & \text{if } |\dot{\gamma}| \geq \dot{\gamma}_c \end{cases} \tag{5}$$

where, $\eta_0 > \eta_1$ and $\dot{\gamma}_c$ is the critical shear rate and $|\dot{\gamma}| = \sqrt{0.5(\dot{\boldsymbol{\gamma}} : \dot{\boldsymbol{\gamma}})}$ is the magnitude of the local symmetrized shear rate tensor. For such systems, an approximation of the lubrication force between a pair of particles immersed in a biviscous matrix under the squeeze mode was derived by Vázquez-Quesada and Ellero [33]. Expanding further, they have provided the analytical results for an apparent slippage effect between two spheres suspended in a biviscous solvent (see Ref. [38]). Inspired by the slip based model of Kroupa et al. [37], they have shown that with properly tuned values of $\dot{\gamma}_c$ and viscosity ratio $\frac{\eta_0}{\eta_1}$, the biviscous description of the matrix can be used to incorporate apparent interparticle slippage effects which could be amongst the physical mechanisms responsible for the shear thinning behavior observed in certain non-Brownian suspensions.

Another utility of the biviscous model is its ability to model apparent yield stress fluids [30] by using a sufficiently low $\dot{\gamma}_c$ and a sufficiently large viscosity ratio. For a given value of the apparent yield stress matrix σ^y_{xy} and viscosity ratio $\frac{\eta_0}{\eta_1}$, an appropriate value of $\dot{\gamma}_c$ can be therefore calculated to regularize the ideal yielding behavior. So, in principle, upon proper

choice of the model parameters in the biviscous fluid two limiting cases can be explored on the rheology of the suspension, that are: (1) interparticle slip effects in a Newtonian matrix or (2) an apparent yield stress matrix. In the following of this section we review the main results in the derivation of the general biviscous lubrication forces.

Consider two spherical particles of radius a_α and a_β moving with a relative normal velocity $V_{\alpha\beta}$ (see Fig. 1). At very close proximities, the surface of the spheres can be considered as paraboloids with an inter-particle gap defined as $h(r) = h_0\left(1 + \frac{r^2}{2\overline{a}h_0}\right)$, where, $\overline{a} = \frac{a_\alpha a_\beta}{a_\alpha + a_\beta}$ and h_0 is the gap at $r = 0$. Through a rigorous derivation, it can be shown that a critical separation distance h_0^{lim} can be defined (see Eqn. (6)), which determines whether the interstitial fluid behaves as monoviscous or biviscous.

$$h_0^{lim} = \frac{3}{4}\sqrt[3]{\frac{9V_{\alpha\beta}^2\overline{a}}{\dot{\gamma}_c^2}} \tag{6}$$

Corresponding expressions for the normal lubrication force of the monoviscous ($F_{\alpha\beta}^m$) and the biviscous ($F_{\alpha\beta}^b$) case are presented in the following.

$$F_{\alpha\beta}^m = 6\pi\eta_0 V\overline{a}^2 h_0^{-1} \quad if\ h_0 \geq h_0^{lim} \tag{7}$$

$$F_{\alpha\beta}^b = 2\pi\left[3\overline{a}^2\eta_0 V_{\alpha\beta}h_0^{-1} + 3\overline{a}^2\left(\eta_0 - \eta_1\right)V_{\alpha\beta}\left\{h^{-1}\left(r_2\right) - h^{-1}\left(r_1\right)\right\}\left[2 - h_0\left\{h^{-1}\left(r_1\right) + h^{-1}\left(r_2\right)\right\}\right]\right.$$
$$\left. + 2\overline{a}\dot{\gamma}_c\left(\eta_0 - \eta_1\right)\left[\left(r_2 - r_1\right) + \left\{h\left(r_1\right) - 2h_0\right\}\sqrt{\frac{2\overline{a}}{h_0}}\left\{arctan\left(\frac{r_2}{\sqrt{2\overline{a}h_0}}\right) - arctan\left(\frac{r_1}{\sqrt{2\overline{a}h_0}}\right)\right\}\right]\right]$$
$$if\ h_0 < h_0^{lim} \tag{8}$$

Here, r_1 and r_2 are the radial co-ordinates which discriminate the spatial regions of the matrix with monoviscosity and biviscosity behavior based on the local shear rate. Their values are calculated as follows:

$$\begin{aligned} r_1 &= r_{max}\left[Q - \sqrt{-3 - Q^2 + 4\left(\frac{\dot{\gamma}_s^{max}}{\dot{\gamma}_c}\right)\frac{1}{Q}}\right], \\ r_2 &= r_{max}\left[Q + \sqrt{-3 - Q^2 + 4\left(\frac{\dot{\gamma}_s^{max}}{\dot{\gamma}_c}\right)\frac{1}{Q}}\right], \end{aligned} \tag{9}$$

where,

$$
\begin{aligned}
r_{max} &= \sqrt{\frac{2\overline{a}h_0}{3}}, \\
\dot{\gamma}_s^{max} &= \frac{9}{8}\frac{V_{\alpha\beta}}{h_0}\sqrt{\frac{3\overline{a}}{2h_0}}, \\
Q &= \sqrt{-1+\frac{1}{P}+P} \quad \text{and} \\
P &= \sqrt[3]{-1+2\left(\frac{\dot{\gamma}_s^{max}}{\dot{\gamma}_c}\right)^2+2\left(\frac{\dot{\gamma}_s^{max}}{\dot{\gamma}_c}\right)\sqrt{\left(\frac{\dot{\gamma}_s^{max}}{\dot{\gamma}_c}\right)^2-1}}.
\end{aligned}
\tag{10}
$$

For more details on the presented model and its derivation, one can refer the original work of Vázquez-Quesada and Ellero [33]. Regarding the consistency between the interparticle lubrication force calculated from a Newtonian fluid model with slip velocity [37] and that derived from the biviscous model equations above, the reader is referred to [38].

C. Computational Domain and other details

To predict the rheological properties, the suspension is subjected to a simple shear test in the three dimensional numerical experiments. A cubic box of size $32a \times 32a \times 32a$ is chosen, with periodic boundaries on all sides except the top and the bottom which are modeled as rigid walls (see Fig. 2). For a chosen value of the input shear rate $\dot{\gamma}_{in}$, the top and the bottom boundaries are assigned a constant value of velocity which drives the flow. The initial particle configuration is setup using a Monte-Carlo method. A linked-list algorithm is used to determine the neighbor particles within a specified distance $rcut_{off}$ that contribute towards the lubrication force acting on a particle. The value of $rcut_{off}$ is set as $2.5a$, such that, the lubrication forces are indeed short-range hydrodynamics forces. To avoid the diverging lubrication forces from stalling the simulation, a $rcut_{on}$ radius is specified, below which the lubrication force between the particles is kept constant. For the present study, the $rcut_{on}$ is set a typical value of $0.001a$ [42]. In addition to the short-range lubrication force, a repulsion force is applied to avoid particle overlapping. The repulsion force takes the following form,

$$
\mathbf{F}_{\alpha\beta}^{rep} = F_0\frac{\tau e^{-\tau h}}{1-e^{-\tau h}}\mathbf{e}_{\alpha\beta} \tag{11}
$$

where, F_0 is its magnitude and τ determines its range. For the present study, hard-sphere repulsion force parameters F_0 and τ are set as 8.4318×10^{-3} and $10^3 a$ respectively. Due to

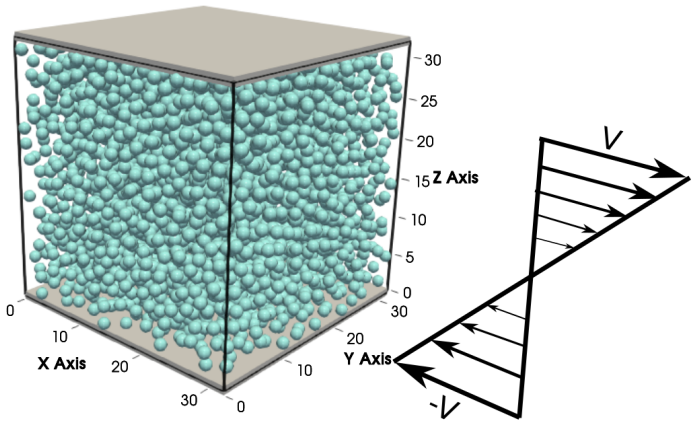

FIG. 2: Schematic of the computational domain. A cubic box of size 32a with periodic boundaries on all sides except top and bottom is considered. The top and bottom boundaries are considered to be walls moving parallel to the x-axis with speed V in opposite directions. The spheres with radius $a = 1$ unit represent the non-Brownian particles that fill the domain interior. Particle volume fractions ranging from 0.05 to 0.48 are considered for the simulations.

the singular nature of the lubrication force, numerical integration of the governing equations using an explicit scheme can impose a serious limitation on the time step size. Hence, an efficient semi-implicit splitting scheme proposed by Vázquez-Quesada and Ellero [22, 23] is implemented to ensure an accurate and stable integration of the equations of motion. According to their approach, the relative velocity of a particle pair $\tilde{\mathbf{V}}_{\alpha\beta}$ can be computed from their previous relative velocity $\mathbf{V}'_{\alpha\beta}$ as follows:

$$\tilde{\mathbf{V}}_{\alpha\beta} = \left(\frac{1}{1 - B_{\alpha\beta}}\right)\left[\mathbf{V}'_{\alpha\beta} + \left(\frac{A_{\alpha\beta} - B_{\alpha\beta}}{1 - A_{\alpha\beta}}\right)\mathbf{V}'_{\alpha\beta} \cdot \mathbf{e}_{\alpha\beta}\mathbf{e}_{\alpha\beta}\right] \tag{12}$$

where, $A_{\alpha\beta}$ and $B_{\alpha\beta}$ are scalar functions defined as,

$$\begin{aligned} A_{\alpha\beta} &= f_{\alpha\beta}(h, rcut_{on}, rcut_{off})\Delta t_{sweep}\left(m_{\alpha}^{-1} + m_{\beta}^{-1}\right) \\ B_{\alpha\beta} &= g_{\alpha\beta}(h, rcut_{on}, rcut_{off})\Delta t_{sweep}\left(m_{\alpha}^{-1} + m_{\beta}^{-1}\right) \end{aligned} \tag{13}$$

that depend on the lubrication model chosen. Here, $m_{\alpha,\beta}$ are the masses of the particles α and β and $\Delta t_{sweep} = \frac{\Delta t}{N_{sweep}}$, is the time step size obtained by splitting Δt with N_{sweep} sub-steps. Since the present pairwise force model obeys the Newton's action-reaction principle,

the velocity of the individual particles can be calculated as,

$$\tilde{\mathbf{V}}_\beta = \frac{m_\alpha \left(\mathbf{V}'_\alpha - \tilde{\mathbf{V}}_{\alpha\beta}\right) + m_\beta \mathbf{V}'_\beta}{m_\alpha + m_\beta} \quad \text{and} \quad \tilde{\mathbf{V}}_\alpha = \tilde{\mathbf{V}}_{\alpha\beta} + \tilde{\mathbf{V}}_\beta. \tag{14}$$

The accuracy of the implicit integration scheme for the lubrication force is highly dependent on the value of N_{sweep}. An adaptive procedure is followed to ensure the value of N_{sweep} is large enough to get convergence while simultaneously being sufficiently small to speed up the calculations. For a default value of N_{sweep} at the n^{th} time step, two different sweeps are performed such that $N_{sweep} = 2^m$ and $N_{sweep} = 2^{m-1}$. Using a L_2 norm defined as,

$$e^m = \frac{\sqrt{\sum_{\alpha=1}^{N} (\tilde{V}_\alpha^m - \tilde{V}_\alpha^{m-1})^2}}{\sqrt{\sum_{\alpha=1}^{N} (\tilde{V}_\alpha^m)^2}} \tag{15}$$

the difference in particles' velocities between the two choice of sweeps is compared with a predefined tolerance ϵ. If $e^m < \epsilon$, then N_{sweep} is halved and the procedure is repeated until $e^{m-q} \geq \epsilon$. Finally, the velocities obtained at $N_{sweep} = 2^{m-q-1}$ are retained and the value of N_{sweep} is set as default for the $n+1$ time step. On the other hand, if $e^m > \epsilon$ the value of N_{sweep} is doubled and the procedure is repeated. Given that the solution converges with 2^{m+q} sweeps, this value is then set as default for the next time step. For all the simulations in this study ϵ was set as 10^{-3}. Once the integration of the lubrication force between all the particle pairs is completed, a Verlet scheme is used to integrate the inter-particle repulsion force. For all simulations, the time step size is chosen as 10^{-4}. For more details on the numerical splitting procedure the reader is referred to Refs. [22] and [23]. The shear rate is generated by imposing a constant velocity to the walls, which are included in the semi-implicit algorithm as spheres of infinite radius. The details of the wall model are given in Appendix VI.

In summary, in the present work an efficient and stable lubrication dynamic simulation is carried out in which short-range hydrodynamic interparticle forces are implicitly taken into account into the pairwise dynamics. In the case of a Newtonian matrix, lubrication contributions follow the classical Eqns. (1) and (2). In the case of a biviscous matrix, only the normal lubrication is considered and hence the suspension rheology is governed by Eqns. (7) and (8). Consistent comparison with the Newtonian case can be done by neglecting high-order logarithmic terms in Eqns. (1) and (2). Note that, unlike FLD-based approaches [25, 26], no self-term particle drag has been included here. On one hand, this bypasses some

complication in the choice of the parameters in FLD, in fact self-terms are selected in FLD to match the mean particle mobility (equivalently the short time self-diffusivity) [43] and usually contains a macroscopic information on the whole suspension, i.e. $\eta(\phi)$ [27] which is one of the output properties of interest. Secondly, we bypass the problem of lack of linear momentum conservation which, in a pairwisely interacting particle system (with antisymmetric forces), is automatically guaranteed.

III. RESULTS AND DISCUSSION

A. Validation study: Rheology of dense non-colloidal suspensions with a Newtonian matrix

To begin with, the viscometric behavior of a non-colloidal suspension with a Newtonian matrix under a simple shear is simulated. This problem has been well documented and therefore serves as an excellent validation study. In a cubical geometry as described in Section II C, the top and bottom walls are moved at a speed of V_z^w in opposite directions along the z-axis to apply an input shear rate $\dot{\gamma}_{in} = V_z^w/16a$. At very large volume fractions, slip can occur at the walls and the suspension may not exhibit a shear rate as defined earlier and therefore an effective shear rate $\dot{\gamma}_{in}^e$ is calculated by interpolating the linear velocity profile in the bulk region. Using the position of the particles and the inter-particle forces, the stress tensor in the bulk region is calculated via the Irving-Kirkwood method [44] as follows:

$$\boldsymbol{\sigma} = \frac{1}{V}\left(\sum_{\alpha} \mathbf{v}_\alpha \mathbf{v}_\alpha + \frac{1}{2}\sum_{\alpha}\sum_{\beta\neq\alpha} \mathbf{r}_{\alpha\beta}\mathbf{F}_{\alpha\beta}\right), \tag{16}$$

where V is the volume of the bulk region, $\mathbf{v}_\alpha$ is the perturbation velocity vector of the particle α, $\mathbf{r}_{\alpha\beta} = \mathbf{r}_\alpha - \mathbf{r}_\beta$ is the relative position vector of the α particle with respect to its β neighbor particle and $\mathbf{F}_{\alpha\beta}$ is the inter-particle force vector. The domain was filled with monodispersed spherical particles of radius $a = 1.0$ using a a Monte-Carlo packing algorithm. For different values of particle volume fraction ranging between 0.05 to 0.45, the number of particles employed varied between 400 to 3500 approximately. Very high values of ϕ are not considered as disorder-to-order transition might occur and contact frictional forces would be significant [45]. Here, we isolate the study to the effect of Newtonian short-range hydrodynamic interactions. Once the simulations reach a steady state, the relative viscosity

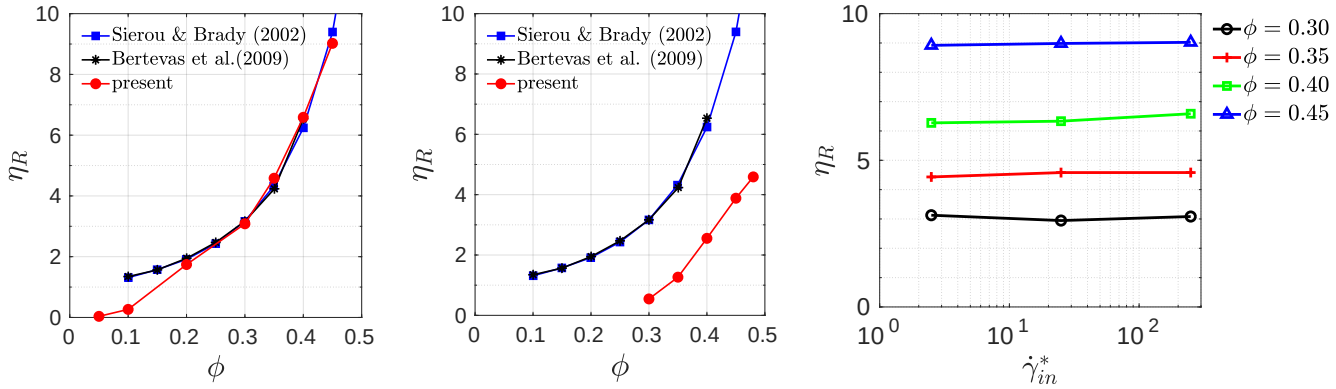

FIG. 3: (a) Variation of η_R with ϕ; results obtained under the combined squeeze and shear mode are shown. (b) Variation of η_R with ϕ; results obtained under squeeze mode alone. In both cases results are compared against data from Sierou and Brady (2002) [45] and Bertevas et al. (2009) [46]. (c) Variation of η_R with the input shear rate ($\dot{\gamma}^*_{in}$) under combined squeeze and shear mode is shown for different particle volume fractions.

of the suspension ($\eta_R = \sigma_{xz}/\eta\dot{\gamma}$) is estimated. Here, η is the viscosity of the suspending medium. By changing the value of the input shear rate, the rheology of the suspension is analyzed based on a non-dimensional shear rate defined as $\dot{\gamma}^*_{in} = \frac{6\pi\eta\bar{a}^2\dot{\gamma}^e_{in}}{F_0}$ [45].

The variation of the relative suspension viscosity with particle volume fraction are plotted in Fig. 3a. In the same figure, the result obtained by Sierou and Brady [45] and Bertevas et al. [46] are co-plotted for validation purpose. In numerical simulations, the short range repulsion force parameters can have significant influence on the rheology of suspensions, especially at higher particle volume fraction. Specifically, the magnitude and the range of the force can alter the micro-structure of the suspended medium, which in turn, alters the suspension viscosity and its shear rate dependence. Therefore, to enable valid comparison, we note that all the results presented in Fig. 3 were obtained for the value of $\tau = 10^3 a$ and $\dot{\gamma}^*_{in} \approx 10^2$. Despite its simplicity, a fairly good prediction of the relative viscosity of the suspension by the present model is clearly evident. For values of particle volume fraction less than 0.3, the relative viscosity of the suspension is under-predicted. This is expected as the inter-particle interactions reduce with particle volume fraction for a fixed value of $rcut_{off}$ and the predicted suspension viscosity falls rapidly to zero as $\phi \to 0$ where no interparticle

lubrication interaction occurs. The variation of the suspension viscosity with $\dot{\gamma}^*_{in}$ is presented in Fig. 3c. As can be seen, a shear-thickening behavior is observed from the simulations. However, the thickening behavior is found to be very mild, particularly for lower volume fractions. A similar observation was also made by Vázquez-Quesada and Ellero [22] who considered the long-range hydrodynamic interactions as well in their simulations.

In the following sections of this paper, we focus on the rheology of dense suspensions with biviscous matrix in which lubrication force under squeeze mode is expected to dominate. Therefore, it is imperative to see whether meaningful predictions are made by the employed model when normal lubrication forces alone in the Newtonian case are considered. To this end, another set of simulations were performed with the same set of parameters as presented before but without considering the tangential lubrication force. The results are presented in Fig. 3b. The variation of the relative suspension viscosity with volume fraction clearly shows an underestimated prediction in the absence of the tangential lubrication and large-range hydrodynamic interactions. Similar constant viscosity values for changing shear rate were observed as in the full case. These results show that the contribution of the normal lubrication alone is clearly insufficient to calculate accurately the viscosity of the suspension. Although the present finding is differing from the work of Ball and Melrose (see Fig. 9 of Ref. [41]), in a more recent study a similar observation was also made by Bertevas et al. [46]. Therefore, especially in shear flows, the tangential lubrication forces do play an important role in suspension behavior. An improvement in the prediction of the relative viscosity using squeeze mode alone was noticed by tuning of the simulation parameters. For example, increasing the value of $rcut_{off}$ enables more neighbor contribution which in turn allows increased dissipation and better prediction of the relative viscosity with normal forces alone. Nevertheless, we did not adopt any such measure and kept the simulation parameter values identical to the combined squeeze and shear-mode simulation run to ensure that the comparisons made were appropriate.

B. Rheology of a dense non-colloidal suspension with a biviscous matrix

In this section, we present the numerical details and the results of the simulation of a dense non-colloidal suspension with a biviscous fluid as matrix. This numerical exercise is

performed to demonstrate the capability of the present biviscosity model to study 1) effect of the apparent slippage (i.e. reproduced via hidden-shear rates effect) on the suspensions rheology and 2) the rheology of a suspension with an apparent yield stress fluid matrix.

1. Effect of apparent slippage on the suspension rheology

When considering dense non-colloidal suspensions with a biviscous matrix, it is essential to account for the short-range lubrication effects. For this purpose, the expressions obtained in [33] that have been briefly reviewed in section II B are used. Using the same problem geometry, flow settings and numerical parameter values as described in Section II C and III A, the suspension rheology of a particulate biviscous fluid with viscosity ratio $\eta_0/\eta_1 = 2.0$ was investigated. To probe the rheology in the dense regime, 3755 monodispersed particles in the cubic box of side 32a ($\phi = 0.48$) was considered. For values of fixed critical shear rate in the range $\dot{\gamma}_c^* = 4.73 \times 10^{-2} - 4.73 \times 10^8$, simulations were performed for different values of input shear rate in the range $\dot{\gamma}_{in}^* = 4.73 - 4.73 \times 10^2$. Once the stresses in the bulk region reached a steady value, the relative suspension viscosity was calculated. Another simulation considering a suspension with a monoviscous Newtonian matrix (with viscosity equal to the high shear viscosity of the biviscous matrix) was carried-out to corroborate the high critical shear rate case ($\dot{\gamma}_c >> \dot{\gamma}$) of the suspension with biviscous matrix.

For different values of the critical shear rate, the obtained relative viscosity is shown in Fig. 4. In the case of $\dot{\gamma}_c^* = 4.73 \times 10^8$ (yellow triangles), the value of the critical shear rate chosen is much higher than the input shear rates and hence the suspension behavior is similar to that of a suspension with a Newtonian ($\eta = \eta_0$) matrix. This is clearly evident from the significant overlapping of the predicted values with the Newtonian case (black circles). Also, a mild shear thickening of the suspension is noticeable which is a distinct feature of a non-colloidal suspension reported in many studies.

In the opposite limit - the $\dot{\gamma}_c^* = 4.73 \times 10^{-2}$ case (red asterisks) - the value of the critical shear rate chosen is much lower than the input shear rates and the suspension once again behaves like a suspension with a Newtonian matrix whose viscosity $\eta = \eta_1$. As expected, a mild shear thickening is observed with the suspension relative viscosities being almost half of the $\dot{\gamma}_c^* = 4.73 \times 10^8$ case. In all other cases, varied levels of shear thinning of the suspension

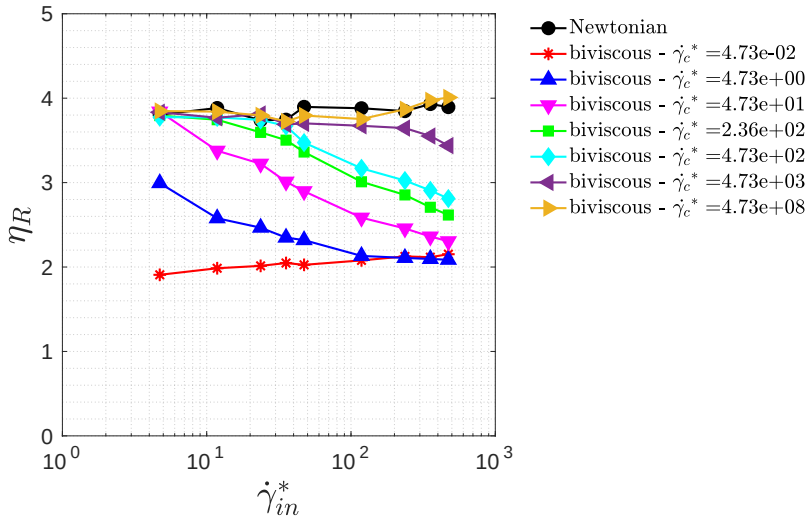

FIG. 4: Results obtained using the biviscous model. Variation of η_R with input shear rate is shown for different values of $\dot{\gamma}_c^*$.

is noticeable depending on the value of the critical shear rate of the matrix.

For a given $\dot{\gamma}_c^*$, the biviscous nature of the suspension itself (i.e. the transition from higher to lower suspension relative viscosity) is found to typically occur at input shear rate much lower than the critical shear rate of the matrix owing to the inter-particle shear rates ($\dot{\gamma}_{loc}^* = \dot{\gamma}_{loc}/\dot{\gamma}_{in}$) locally exceeding the critical shear rate of the matrix. Moreover, as shown in Fig. 5, for the same critical shear rate $\dot{\gamma}_c^* = 4.73 \times 10^3$ of the biviscous matrix, an increase of the viscosity ratio to $\frac{\eta_0}{\eta_1} = 10$ enhances the resulting thinning behaviour of the suspension anticipating it to lower values of the applied shear rate. The previous results reproduce the ones obtained by Vázquez-Quesada et al. [5, 28] with a different shear-thinning matrix and show that the 'hidden' high shear rates come into play, resulting in a shear-thinning of the suspension at the macroscopic level.

From Fig. 4 it is also evident that if $\dot{\gamma}_c$ is extremely large (as for example in a truly Newtonian matrix such as glycerol), no shear-thinning of the suspension is obtained which contrasts experimental observations [5]. However, as discussed in Ref. [38], even in the case of Newtonian matrices (provided that slip occurrs in interparticle gaps) the parameter $\dot{\gamma}_c$ can be practically chosen much smaller than the true rheological value. Since this choice leads to shear thinning in the suspension, it strengthen the hypothesis put forward by Kroupa et al. in [37] of interparticle slippage as a possible additional cause of shear-thinning in suspensions

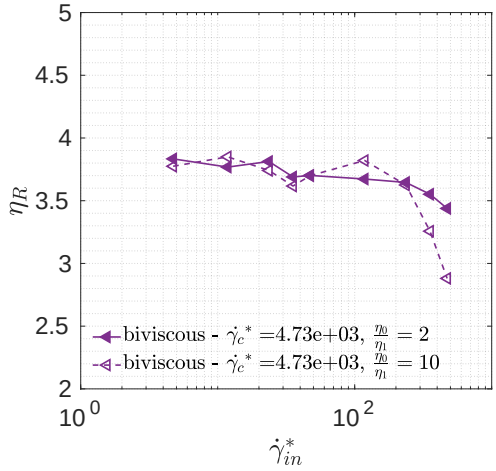

FIG. 5: For two different viscosity ratios $\frac{\eta_0}{\eta_1}$, namely 2 and 10, the variation of η_R with input shear rate is shown for the case of $\dot{\gamma}^*_c = 4.73 \times 10^3$.

with constant-viscosity matrices.

It should be clear from Eqns. (7) and (8) that the shear rate dependent monoviscous or biviscous behavior of the interstitial fluid between a pair of particles has been reformulated into inter-particle separation-based behavior. Specifically, when the inter-particle separation between a particle pair is less than h_0^{lim}, the local shear rate exceeds the critical shear rate of the matrix and the expression for biviscous lubrication force is appropriately used. It should be noted that the value of h_0^{lim} depends not only $\dot{\gamma}_c$ but also on the relative velocity of the particles. For all the values of critical shear rate studied, the fraction of particle pairs under biviscous interation is shown for different input shear rates in Fig. 6. Across the range of input shear rate studied, the $\dot{\gamma}^*_c = 4.73 \times 10^8$ case shows that all interactions are monoviscous, whereas, in the case of $\dot{\gamma}^*_c = 4.73 \times 10^{-2}$ and all other intermediate cases, interactions are found to be biviscous in nature. As discussed earlier, a significant fraction of particle pairs experience biviscous interaction locally i.e. $\dot{\gamma}^*_{loc} > \dot{\gamma}^*_c$ well before the global condition $\dot{\gamma}^*_{in} > \dot{\gamma}^*_c$ is satisfied. This can be seen clearly by comparison of Figs. 4 and 6 in the case of $\dot{\gamma}^*_c = 4.73 \times 10^3$, where the suspension shear-thinning begins at $\dot{\gamma}^*_{in} \approx 10^2 << \dot{\gamma}^*_c$, where around 20% of the interactions are bi-viscous. With systematic reduction in the value of $\dot{\gamma}^*_c$, a monotonous increase in the fraction of biviscous interaction is observed in the investigated parametric space.

To further delineate the transition from mono to biviscous state of the suspension, the

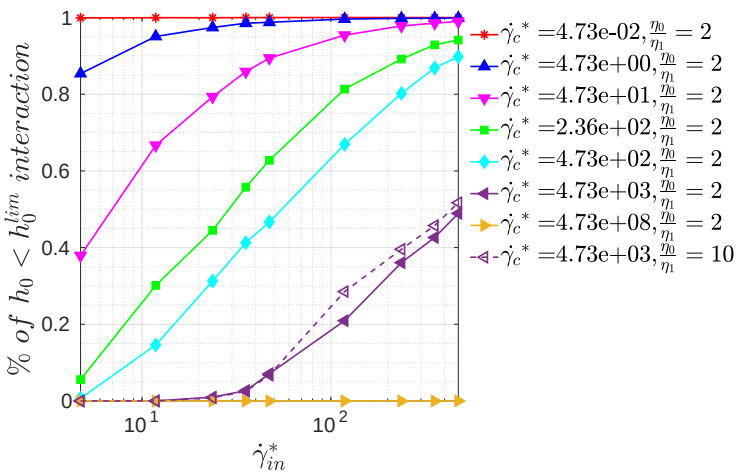

FIG. 6: For different values of critical shear rate, the transition from high shear viscosity to low shear viscosity is shown in terms of percentage of interaction for which the inter-particle distance h_0 less than the critical value h_0^{lim}.

inter-particle shear rate (Eq. (17)) for all the particle pairs are plotted against their inter-particle separation in Fig. 7.

$$\dot{\gamma}_{loc} = \frac{9V_{\alpha\beta}}{8h_0}\sqrt{\frac{3a}{2h_0}} \tag{17}$$

The columns show the variation for change in the value of critical shear rate and the rows for change in input shear rate. The data points marked in blue and red indicate monoviscous and biviscous interaction respectively. From the plots, it is clearly seen that the shear rate in the fluid domain can locally exceed the input shear rate. Progressively larger shear rates are found with decreasing inter-particle gap. As the inter-particle gap should decrease with larger input shear rate, the probability of biviscous interaction should increase for higher $\dot{\gamma}_{in}^*$ for a particular value of $\dot{\gamma}_c^*$. This expected behavior is clearly seen when going from left to right in the rows of Fig. 7. With a decrease in the value of $\dot{\gamma}_c^*$, the number of interactions wherein the interstitial fluid has shear thinned can be seen to substantially increase. This transition can be found to be accelerated by increasing the value of input shear rate (see columns 2 and 3 in Fig. 7). The horizontal interface-like line seen between the two different types of interaction (in rows 2 and 3) corroborates the usage of a fixed value of critical shear rate in the simulations. It is also evident from these results that the transition occurs at any value of inter-particle separation as the h_0^{lim} is also a function of the relative velocity of the interacting particle pair.

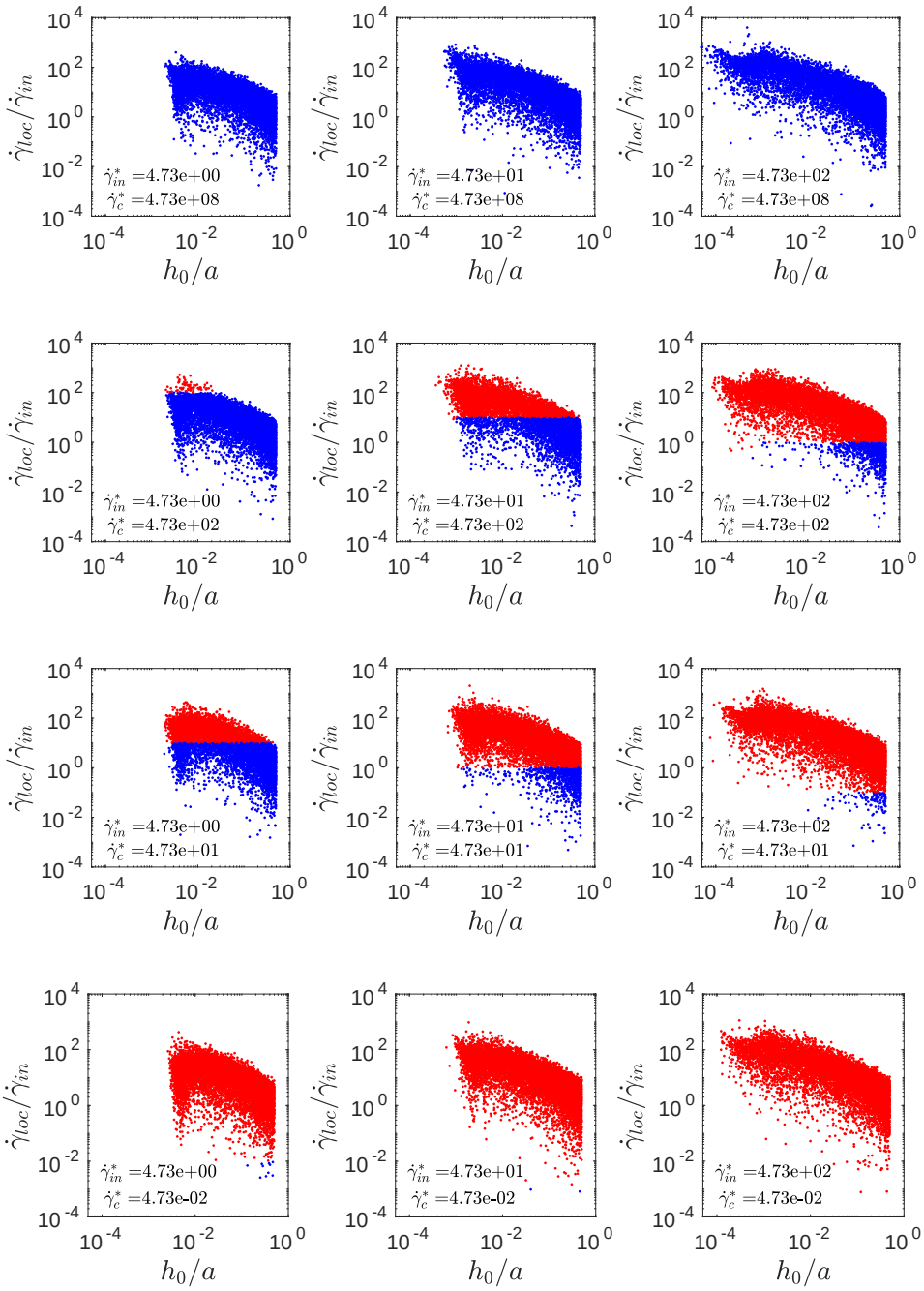

FIG. 7: Variation of the inter-particle shear rate with inter-particle separation is shown for different values of critical shear rate (rows) and input shear rate (columns). The blue and red dots represent monoviscous and biviscous interactions respectively.

2. *Rheology of a suspension with a yield stress fluid*

As previously discussed, the biviscosity model is one of the many techniques that can be used for the regularization of the Bingham model describing ideal viscoplastic/yield stress fluids. A schematic of the one dimensional rheology of a biviscous fluid is shown in Fig. 8(a). The fluid is characterized by low-shear viscosity (η_0) that is much larger than the high-shear viscosity (η_1). The shear rate at which the transition of the fluid's viscosity from η_0 to η_1 occurs is termed as the critical shear rate $\dot{\gamma}_c$. This description of an ideal biviscous fluid can be suitably adapted to simulate an apparent yield stress fluid. As shown in Fig. 8(b), by setting a sufficiently low value for $\dot{\gamma}_c$, the transition from low to high-shear viscosity approximates a plastic deformation occurring at a finite value of shear stress resembling a yield stress. Using this approach, the Bingham model with discontinuous conditions can be regularized through a set of piecewise continuous conditions, which represent the real viscoplastic fluids when neglecting the other material behaviors such as elasticity that could be in play.

With a similar setup as presented in the previous section, we carry out the lubrication dynamics-based simulation of a non-colloidal suspension with a pseudo yield stress fluid as the solvent. Using the biviscous model, the simulation parameters required to mimic the yielding behavior of the matrix are determined as follows. Firstly, the range of Bingham number (Bn), defined as the ratio between the yield stress σ_s^y to the stress scale $\eta_1\dot{\gamma}_{in}$ of the matrix, typically probed in the experimental works was found. Based on the work of Ovarlez et al. [4], the range for Bingham number to be studied in the present work was

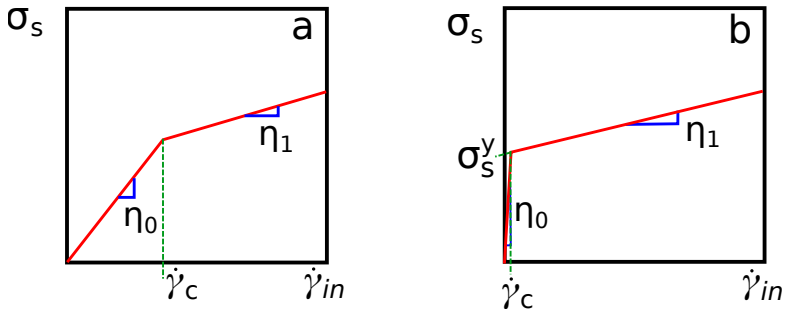

FIG. 8: Schematic of a one-dimensional rheology of a biviscous fluid using the a) biviscous model and b)and its modification ($\dot{\gamma}_c << 1$) to represent an apparent yield stress fluid. The extrapolation of the flow curve to $\dot{\gamma}_{in} \to 0$ defines the apparent yield stress $\sigma_s^y = (\eta_0 - \eta_1)\dot{\gamma}_c$.

chosen to range across $\mathcal{O}(10^{-1})$ and $\mathcal{O}(10^{1})$. By setting the extrapolated solvent yield stress $\sigma_s^y = 0.1Pa$, solvent plastic viscosity $\eta_1 = 8.46Pa.s$ and the input shear rate in the range $2.5 \times 10^{-4}s^{-1}$ to $5 \times 10^{-2}s^{-1}$, the value of Bn for the present study varies between 0.2 to 47.28. With the values of the yield stress and plastic viscosity of the matrix fixed in order to ensure the continuity of the stress function for all shear rates, the value of η_0 for the biviscous model uniquely depends on the value of the critical shear rate $\dot{\gamma}_c$. For the present study, $\dot{\gamma}_c$ is set as $10^{-3}s^{-1}$ and the corresponding value of the viscosity ratio η_0/η_1 is found to be 12. As in the previous section, monodispersed spherical particles were randomly arranged using a Monte Carlo method such that particle volume fraction $\phi = 0.48$.

Using a homogenization approach, Ovarlez et al.[4] provided the analytical estimate of the suspension properties for systems with a yield stress fluid as the solvent. Here, the same approach is followed to determine the suspension properties at any given particle volume fraction. For a biviscous matrix, the apparent viscosity can be found to be $\eta_b(\dot{\gamma}_{in}) = (\sigma_s^y + \eta_1\dot{\gamma}_{in})/\dot{\gamma}_{in}$, for $\dot{\gamma}_{in} \geq \dot{\gamma}_c$. Then, the shear stress in a non-colloidal suspension with a biviscous matrix under a simple shear can be expressed as,

$$\sigma = g(\phi)\eta_b(\dot{\gamma}_{in})\dot{\gamma}_{in} \tag{18}$$

where, $g(\phi)$ is the parameter that takes into account the influence of the suspension microstructure and the local shear rate. Based on the density of energy dissipated at the interstitial fluid region, it was shown that an estimate for local shear rate can be expressed as, $\bar{\dot{\gamma}}_{loc}(\phi) = \dot{\gamma}_{in}\sqrt{g(\phi)/(1-\phi)}$ [4]. Using this estimate to account for local shear rate effects on the apparent viscosity of the biviscous matrix, Eqn. (18) can be rewritten as,

$$\begin{aligned}
\sigma &= g(\phi)\eta_b(\bar{\dot{\gamma}}_{loc}(\phi))\dot{\gamma}_{in} \\
&= \sqrt{(1-\phi)g(\phi)}\left[\sigma_s^y + \eta_1\sqrt{\frac{g(\phi)}{1-\phi}}\dot{\gamma}_{in}\right] \\
&= \sigma^y(\phi) + \eta(\phi)\dot{\gamma}_{in}
\end{aligned} \tag{19}$$

where, $\sigma^y(\phi)$ and $\eta(\phi)$ represents the suspension yield stress and suspension plastic viscosity at a given particle volume fraction. Therefore, the non-dimensional yield stress and the non-dimensional consistency of the suspension are obtained as follows,

$$\frac{\sigma^y(\phi)}{\sigma_s^y} = \sqrt{(1-\phi)g(\phi)} \tag{20}$$

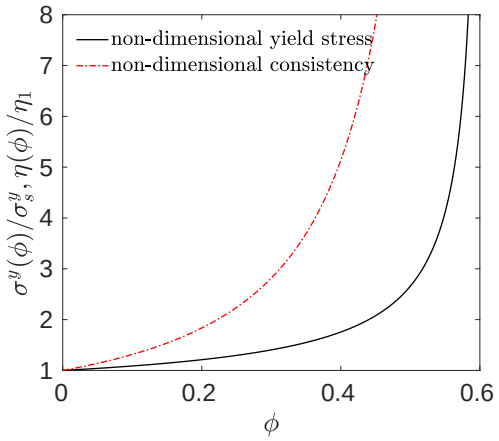

FIG. 9: Variation of the dimensionless yield stress and consistency with particle volume fraction for a non-colloidal suspension with biviscous matrix obtained using the homogenization theory of Overlaz et al. [4].

$$\begin{aligned} \frac{\eta(\phi)}{\eta_1} &= g(\phi) \\ &= \frac{1}{1-\phi}\left(\frac{\sigma^y(\phi)}{\sigma_s^y}\right)^2 \end{aligned} \tag{21}$$

For the case of anisotropic suspensions, the parameter $g(\phi)$ in the above equations could be estimated based on the Krieger-Dougherty equation,

$$g(\phi) = (1-\phi/\phi_{div})^{-2.5\phi_{div}} \tag{22}$$

with $\phi_{div} = 0.605$. When the biviscous model is employed for the solvent, it can be noticed that the non-dimensional consistency for a non-colloidal suspension follows the Krieger-Dougherty equation. On the other hand, the expression for the non-dimensional yield stress remains the same, irrespective of whether the Bingham, Herschel-Bulkley or biviscous description is used to model a yield stress fluid matrix. For a non-colloidal suspension with biviscous matrix, the variation of the dimensionless yield stress and consistency with particle volume fraction are shown in Fig. 9.

For the range of input shear rate specified earlier, simulations were performed for a suspension with particle volume fraction $\phi = 0.48$. The variation of the shear stress in the suspension ($\sigma(\dot{\gamma}, \phi = 0.48)$) with the input shear rate is shown in Fig. 10. For low shear rates, vanishingly small values of the shear stress are observed. Moreover, as the input shear rate exceeds the critical shear rate and increases to larger values, the inter-particle separation

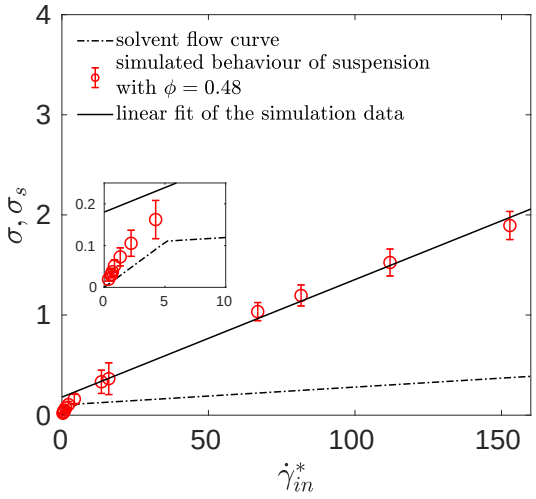

FIG. 10: Variation of the suspensions shear stress with the input shear rate is shown for the $\phi = 0.48$ case.

h_0 becomes lower than the value of h_0^{lim} causing the transition of the solvent viscosity from η_0 to η_1, i.e. from monoviscous (unyielded) to biviscous (yielded) behavior [33] (see Fig. 11). With the increase in the fluidity of the solvent, the bulk shear stress of the suspension is then found to grow more rapidly with the input shear rate. The variation of the shear stress of the solvent (σ_s), calculated using the biviscous model, with the input shear rate is co-plotted in Fig. 10 to highlight the significant contribution of the suspended particles to the bulk shear stress.

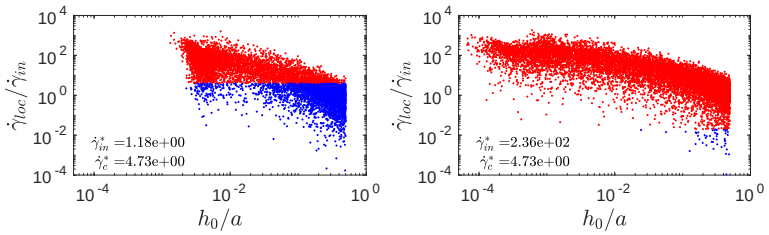

(a)

FIG. 11: For the yield stress calculations, $\dot{\gamma}^*_c$ was set a low value of 4.73. The local inter-particle shear rates are compared for two input shear rates $\dot{\gamma}^*_{in} = 1.18$ and 2.36×10^2. Blue and red colors correspond respectively to particle pairs interacting via monoviscous (unyielded) and biviscous (yielded) lubrication forces.

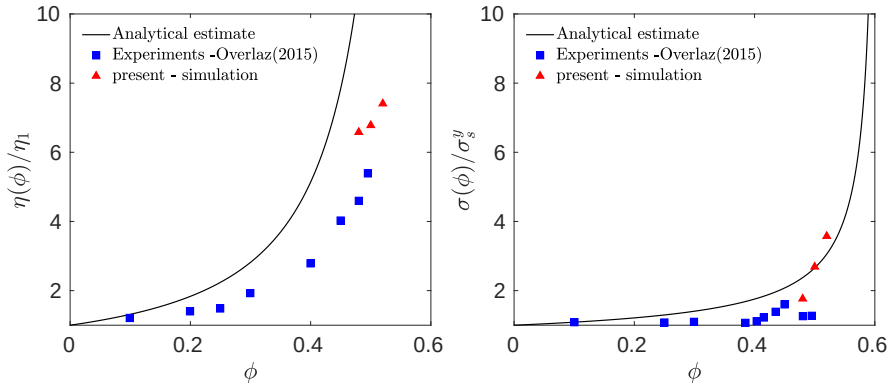

(a) (b)

FIG. 12: Comparison of non-dimensional consistency and yield stress values from the present simulations against the analytical and experimental results.

From the linear fit of the simulation data, the apparent yield stress and the viscosity of the suspension is obtained as $0.176Pa$ and $55.67Pa.s$ (Fig. 10). The predicted non-dimensional yield stress and consistency are therefore found to be 1.76 and 6.58 respectively. For comparison purpose, the analytical values from the homogenization theory presented earlier and the experimental estimates from the work of Ovarlez et al. [4] are used. Eqns. (20) and (21) provides the analytical values of non-dimensional yield stress and consistency for $\phi = 0.48$ as 2.37 and 10.86 respectively. In addition, the experimental values for the non-dimensional yield stress and consistency from Ref. [4] are 1.27 and 5.39 approximately. It should be pointed out that the experimental values were obtained through a Herschel-Bulkley fit of the flow curve and therefore direct comparison with the analytical estimate of the dimensionless consistency from the biviscous model cannot be made. Under this circumstance, the Herschel-Bulkley model based analytical estimate for non-dimensional consistency, $\frac{\eta_{HB}(\phi)}{\eta_{HB}} = 6.13$, should be used. However, the analytical estimate of the non-dimensional yield stress remains the same for both the biviscous and Herschel-Bulkley models, allowing direct comparisons to be made. As we have considered only the squeeze mode for the inter-particle lubrication interactions, the dimensionless yield stress predicted from the simulation (red triangles), when compared with the analytical estimates, are found to be underestimated (Fig. 12b). However, they are slightly larger than the experimental values (blue squares). In a similar manner, the dimensionless consistency from the simulation is smaller than the analytical estimates ob-

tained using the biviscosity model Fig. (12a). Nevertheless, it is significantly higher than the experimental and analytical estimates, obtained using the Herschel-Bulkley model, from the work of Ovarlez et al. [4]. Since the squeeze mode alone is employed, for lower values of particle volume concentration (for $\phi < 0.48$) the bulk did not achieve the prescribed input shear rates and hence the suspension properties could not be predicted. However, at higher volume fractions ($\phi = 0.50$ and 0.52) significant yielding of the suspension could be achieved.

Since the suspension properties are largely influenced by its microstructure, it is necessary to examine the spatial distribution of the particles in the bulk. This is achieved by analyzing the radial distribution function (RDF) of the particle system after the macroscopic shear rate of the suspension has reached a steady value. Fig. 13 shows the RDF in the velocity-velocity gradient$(x - z)$ plane obtained from the present simulation. Figs. 13a and 13b shows the RDFs at two different input rates, $\dot{\gamma}^*_{in} = 1.18$ and 2.36×10^2 respectively, one above and below the critical shear rate of the solvent. Although, the RDFs are noticeably different from each other, some similarities are observable such as the broken fore-aft symmetry. As expected in a simple shear flow, at both shear rates, an increased probability of finding particle-pairs at very close separations is observed along the compression axis. To balance this, particle depletion is found to occur along the extension axis but not always in an orthogonal direction to the compression axis. As the details of anisotropic particle distribution depend on the shear rate, the RDFs in polar coordinates is presented in Fig. 13c for more clarity. Specifically, the probability of finding a particle pair with inter-particle separations close to the diameter of the particles alone is shown. In the low $\dot{\gamma}^*_{in}$ case, the maxima are found to be along the angles 120° and 300°, whereas the minima are found to be orthogonal to the maxima along the angles 30° and 210°. In the high $\dot{\gamma}^*_{in}$ case, the maxima are found to be along the angles 170° and 350°, and the minima along the angles 30° and 210°. While regions of particle depletion seem to be roughly the same at high and low shear rates, there is a significant difference in the region of particle accumulation which tends to move closer to the flow direction. Distinctive secondary maxima and minima are found in the high shear rate case along the 90° and 270° angles. This 'tail' formation is in good agreement with the experimental results of Ovarlez et al.[4] determined using the X-ray microtomography. Overall, the microstructure predicted by the present simulation methodology is in fairly good agreement with the experiments. In

particular, the shear rate dependency of the microstructure in suspensions with viscoplastic matrix is clearly brought out.

IV. SUMMARY AND CONCLUSION

In this paper, a numerical approach to predict the rheology of a non-colloidal suspension with a biviscous matrix was presented. Using the lubrication dynamics based on the

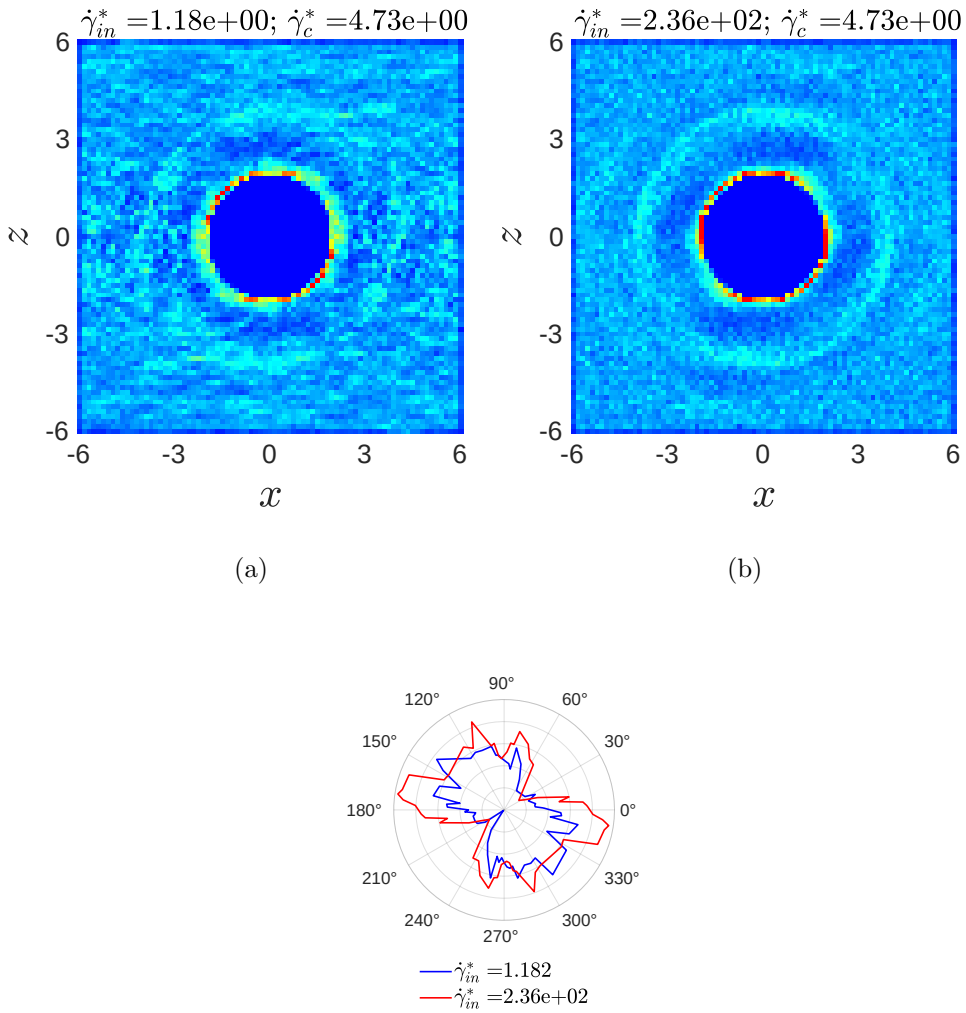

(a) (b)

(c)

FIG. 13: RDF on the $x-z$ plane for a) $\dot{\gamma}^*_{in} = 1.18$ and b) $\dot{\gamma}^*_{in} = 2.36 \times 10^2$ are shown. c) The probability distribution function in a polar plot for particle-pair distance $r_{\alpha\beta}$ in the range of 2.001 to 2.04.

biviscosity model, behavior of suspensions with matrices which undergo shear thinning at low and high shear rates was studied. Firstly, the decrease in the viscosity of concentrated suspensions of non-colloidal particles with shear rate due to an apparent slip of the solvent on the particles surface (which is explained in terms of the high-shear rheology of the biviscous matrix) was demonstrated by setting larger values for the critical shear rate. The variation of the shear stress in the interstitial fluid regions between the particles with the input shear rate were presented to elucidate the influence of the apparent slippage on the suspension relative viscosity. With increasing proportion of fluid slippage (modeled as the shear rate dependent transition from high to low value of the matrix viscosity) in the inter-particle gaps, a corresponding decrease in the suspension relative viscosity was observed. The crucial message here is that the presence of interparticle slippage effectively lowers the value of critical shear rate used in the biviscous model which does not need to be equal to the true rheological one in the real matrix. These results further reinforce the findings of Kroupa et al.[37] and Vázquez-Quesada et al. [38] supporting the idea that shear-thinning in suspensions with Newtonian constant-viscosity matrices can be alternatively explained in terms of an interparticle apparent slip.

Secondly, by setting a low value for the critical shear rate, the rheology of a suspension with an apparent yield stress fluid is presented. The predictive capability of the proposed numerical approach based on the biviscosity description of a yield stress matrix was found to be particularly good only at high volume fractions. At moderate volume fractions the shear mode inter-particle lubrication force could significantly contribute and cannot be neglected. Considering only the squeeze mode, the numerical prediction of the suspension relative viscosity, yield stress and microstructure of the suspension was found to compare well with the experiments and the analytical estimates. In particular, the predicted shear rate dependency of the microstructure corroborates the experimental findings of Ovarlez et al.[4]. The present model can be extended to the simulation of dense non-colloidal suspension interacting with a discontinuous shear-thickening medium (e.g. another concentrated colloidal dispersion [47]). In this case analytical interparticle lubrication expressions based on an inverse biviscous model have been recently derived in [48] and can be straightforwardly incorporated into the the present computational framework.

V. ACKNOWLEDGEMENTS

This research is supported by the Basque Government through the BERC 2018- 2021 programme and by the Spanish State Research Agency through BCAM Severo Ochoa excellence accreditation SEV-2017-0718 and through project RTI2018-094595- B-I00 funded by (AEI/FEDER, UE) and acronym VIRHACOST. The authors acknowledge also the financial support received by the Basque Business Development Agency under ELKARTEK 2019 programme (MATHEO project: grant KK-2019/00085).

VI. APPENDIX: MODELING OF THE WALL BOUNDARIES

To impose the wall boundary conditions on the top and bottom surfaces of the problem domain the following approach is adopted. When a suspension particle of radius a and velocity $\boldsymbol{V}$ is within the $rcut_{off}$ distance from the a wall moving at velocity $\boldsymbol{V}_w$, the normal and tangential forces exerted on the suspension particle is given by [49, 50]

$$\begin{aligned} \boldsymbol{F}^n_{\alpha w} &= f_{\alpha w}(\boldsymbol{V}_\alpha - \boldsymbol{V}_w)\cdot \boldsymbol{e}_{\alpha w}\boldsymbol{e}_{\alpha w} \\ \boldsymbol{F}^t_{\alpha w} &= g_{\alpha w}(\boldsymbol{V}_\alpha - \boldsymbol{V}_w)\cdot (\boldsymbol{1} - \boldsymbol{e}_{\alpha w}\boldsymbol{e}_{\alpha w}) \end{aligned} \tag{23}$$

where

$$\begin{aligned} f_{\alpha w} &= -6\pi\eta a\left\{\frac{a}{h} + \frac{1}{5}ln\left(\frac{a}{h}\right) + k\right\} \\ g_{\alpha w} &= -\frac{16}{5}\pi\eta a ln\left(\frac{a}{h}\right) \end{aligned} \tag{24}$$

Here, k is a suitable constant taken as 0.971264. To solve for the particle velocity using the semi-implicit scheme, for every particle-wall pair, their final velocities $\tilde{\boldsymbol{V}}_\alpha$ are written in terms of the previous velocities $\boldsymbol{V}'_\alpha$ as

$$\tilde{\boldsymbol{V}}_\alpha = \boldsymbol{V}'_\alpha + \tilde{\boldsymbol{F}}_{\alpha w}\frac{\Delta t_{sweep}}{m_\alpha} \tag{25}$$

$$\tilde{\boldsymbol{V}}_w = \boldsymbol{V}'_w = \boldsymbol{V}_w \tag{26}$$

Subtracting Eqns. (25) and (26), and substituting Eqn. (23), we get

$$\tilde{\boldsymbol{V}}_{\alpha w}\cdot\left\{\left(g_{\alpha w} - f_{\alpha w}\right)\boldsymbol{e}_{\alpha w}\boldsymbol{e}_{\alpha w} + (1 - g_{\alpha w})\boldsymbol{1}\right\}\frac{\Delta t_{sweep}}{m_\alpha} = \boldsymbol{V}'_{\alpha w} \tag{27}$$

for which the solution is

$$\tilde{\boldsymbol{V}}_\alpha = \boldsymbol{V}_w + \left(\frac{1}{1-B_{\alpha w}}\right)\boldsymbol{V}'_{\alpha w}\cdot\left\{\mathbf{1} + \left(\frac{A_{\alpha w}-B_{\alpha w}}{1-B_{\alpha w}}\right)\boldsymbol{e}_{\alpha w}\boldsymbol{e}_{\alpha w}\right\} \tag{28}$$

where

$$\begin{aligned} A_{\alpha w} &= f_{\alpha w}\Delta t_{sweep}/m_\alpha \\ B_{\alpha w} &= g_{\alpha w}\Delta t_{sweep}/m_\alpha. \end{aligned} \tag{29}$$

REFERENCES

[1]W. R. Hwang, M. A. Hulsen, and H. E. Meijer, "Direct simulations of particle suspensions in a viscoelastic fluid in sliding bi-periodic frames," Journal of Non-Newtonian Fluid Mechanics **121**, 15 – 33 (2004).

[2]N. S. Martys, W. L. George, B.-W. Chun, and D. Lootens, "A smoothed particle hydrodynamics-based fluid model with a spatially dependent viscosity: application to flow of a suspension with a non-newtonian fluid matrix," Rheologica Acta **49**, 1059–1069 (2010).

[3]M. Liard, N. S. Martys, W. L. George, D. Lootens, and P. Hebraud, "Scaling laws for the flow of generalized newtonian suspensions," Journal of Rheology **58**, 1993–2015 (2014), https://doi.org/10.1122/1.4896896.

[4]G. Ovarlez, F. Mahaut, S. Deboeuf, N. Lenoir, S. Hormozi, and X. Chateau, "Flows of suspensions of particles in yield stress fluids," Journal of Rheology **59**, 1449–1486 (2015), https://doi.org/10.1122/1.4934363.

[5]A. Vázquez-Quesada, A. Mahmud, S. Dai, M. Ellero, and R. I. Tanner, "Investigating the causes of shear-thinning in non-colloidal suspensions: Experiments and simulations," Journal of Non-Newtonian Fluid Mechanics **248**, 1–7 (2017).

[6]D. Alghalibi, I. Lashgari, L. Brandt, and S. Hormozi, "Interface-resolved simulations of particle suspensions in newtonian, shear thinning and shear thickening carrier fluids," Journal of Fluid Mechanics **852**, 329357 (2018).

[7]M. Yang and E. S. G. Shaqfeh, "Mechanism of shear thickening in suspensions of rigid spheres in boger fluids. part ii: Suspensions at finite concentration," Journal of Rheology **62**, 1379–1396 (2018), https://doi.org/10.1122/1.5024698.

[8]A. Vázquez-Quesada, P. Español, R. I. Tanner, and M. Ellero, "Shear thickening of a non-colloidal suspension with a viscoelastic matrix," Journal of Fluid Mechanics **880**, 10701094 (2019).

[9]R. Seto, R. Mari, J. F. Morris, and M. M. Denn, "Discontinuous shear thickening of frictional hard-sphere suspensions," Phys. Rev. Lett. **111**, 218301 (2013).

[10]R. Mari, R. Seto, J. F. Morris, and M. M. Denn, "Shear thickening, frictionless and frictional rheologies in non-brownian suspensions," Journal of Rheology **58**, 1693–1724 (2014), https://doi.org/10.1122/1.4890747.

[11]G. DAvino, P. Maffettone, M. Hulsen, and G. Peters, "A numerical method for simulating concentrated rigid particle suspensions in an elongational flow using a fixed grid," Journal of Computational Physics **226**, 688 – 711 (2007).

[12]A. Wachs, A. Hammouti, G. Vinay, and M. Rahmani, "Accuracy of finite volume/staggered grid distributed lagrange multiplier/fictitious domain simulations of particulate flows," Computers & Fluids **115**, 154 – 172 (2015).

[13]S. Krishnan, E. S. Shaqfeh, and G. Iaccarino, "Fully resolved viscoelastic particulate simulations using unstructured grids," Journal of Computational Physics **338**, 313 – 338 (2017).

[14]A. R. Koblitz, S. Lovett, and N. Nikiforakis, "Direct numerical simulation of particle sedimentation in a bingham fluid," Phys. Rev. Fluids **3**, 093302 (2018).

[15]N. Trask, M. Maxey, K. Kim, M. Perego, M. L. Parks, K. Yang, and J. Xu, "A scalable consistent second-order sph solver for unsteady low reynolds number flows," Computer Methods in Applied Mechanics and Engineering **289**, 155 – 178 (2015).

[16]N. Trask, M. Maxey, and X. Hu, "A compatible high-order meshless method for the stokes equations with applications to suspension flows," Journal of Computational Physics **355**, 310 – 326 (2018).

[17]W. Hu, N. Trask, X. Hu, and W. Pan, "A spatially adaptive high-order meshless method for fluidstructure interactions," Computer Methods in Applied Mechanics and Engineering **355**, 67 – 93 (2019).

[18]A. Sierou and J. F. Brady, "Accelerated stokesian dynamics simulations," Journal of Fluid Mechanics **448**, 115146 (2001).

[19]A. M. Fiore and J. W. Swan, "Fast stokesian dynamics," Journal of Fluid Mechanics **878**, 544597 (2019).

[20]N. S. Martys, "Study of a dissipative particle dynamics based approach for modeling suspensions," Journal of Rheology **49**, 401–424 (2005), https://doi.org/10.1122/1.1849187.

[21]A. J. C. Ladd and R. Verberg, "Lattice-boltzmann simulations of particle-fluid suspensions," Journal of Statistical Physics **104**, 1191–1251 (2001).

[22]A. Vázquez-Quesada and M. Ellero, "Rheology and microstructure of non-colloidal suspensions under shear studied with smoothed particle hydrodynamics," Journal of Non-Newtonian Fluid Mechanics **233**, 37 – 47 (2016), papers presented at the Rheology Symposium in honor of Prof. R. I. Tanner on the occasion of his 82nd birthday, in Vathi, Samos, Greece.

[23]X. Bian and M. Ellero, "A splitting integration scheme for the sph simulation of concentrated particle suspensions," Computer Physics Communications **185**, 53 – 62 (2014).

[24]A. Vázquez-Quesada, X. Bian, and M. Ellero, "Three-dimensional simulations of dilute and concentrated suspensions using smoothed particle hydrodynamics," Computational Particle Mechanics **3**, 167–178 (2016).

[25]A. Kumar and J. J. L. Higdon, "Origins of the anomalous stress behavior in charged colloidal suspensions under shear," Phys. Rev. E **82**, 051401 (2010).

[26]D. S. Bolintineanu, G. S. Grest, J. B. Lechman, F. Pierce, S. J. Plimpton, and P. R. Schunk, "Particle dynamics modeling methods for colloid suspensions," Computational Particle Mechanics **1**, 321–356 (2014).

[27]A. K. Townsend and H. J. Wilson, "Anomalous effect of turning off long-range mobility interactions in stokesian dynamics," Physics of Fluids **30**, 077103 (2018), https://doi.org/10.1063/1.5031860.

[28]A. Vázquez-Quesada, R. I. Tanner, and M. Ellero, "Shear thinning of noncolloidal suspensions," Phys. Rev. Lett. **117**, 108001 (2016).

[29]S. Kim and S. Karrila, *Microhydrodynamics: Principles and Selected Applications*, Butterworth - Heinemann series in chemical engineering (Dover Publications, 2005).

[30]R. I. Tanner and J. F. Milthorpe, "Numerical simulation of the flow of fluids with yield stress," in *Num Meth Lam Turb Flow (Eds Taylor C, Johnson JA, Smith WR)*, Proc 3rd Int Conf (Seattle) (Pineridge Press, Swansea, 1983) pp. 680–690.

[31]R. B. Bird, G. C. Dai, and B. J. Yarusso, "The rheology and flow of viscoplastic materials," Reviews in Chemical Engineering **1**, 1–70 (2016).

[32]T. C. Papanastasiou, "Flows of materials with yield," Journal of Rheology **31**, 385–404 (1987), https://doi.org/10.1122/1.549926.

[33]A. Vázquez-Quesada and M. Ellero, "Analytical solution for the lubrication force between two spheres in a bi-viscous fluid," Physics of Fluids **28**, 073101 (2016), https://aip.scitation.org/doi/pdf/10.1063/1.4954815.

[34]C. R. Beverly and R. I. Tanner, "Numerical analysis of extrudate swell in viscoelastic materials with yield stress," Journal of Rheology **33**, 989–1009 (1989), https://doi.org/10.1122/1.550042.

[35]Prashant and J. Derksen, "Direct simulations of spherical particle motion in bingham liquids," Computers & Chemical Engineering **35**, 1200 – 1214 (2011).

[36]H. A. Barnes, "The yield stress - a review or '$\pi\alpha\nu\tau\alpha$ $\rho\epsilon\iota$' - everything flows?" Journal of Non-Newtonian Fluid Mechanics **81**, 133 – 178 (1999).

[37]M. Kroupa, M. Soos, and J. Kosek, "Slip on a particle surface as the possible origin of shear thinning in non-brownian suspensions," Phys. Chem. Chem. Phys. **19**, 5979–5984 (2017).

[38]A. Vázquez-Quesada, P. Español, and M. Ellero, "Apparent slip mechanism between two spheres based on solvent rheology: Theory and implication for the shear thinning of non-brownian suspensions," Phys. Rev. Fluids **3**, 123302 (2018).

[39]A. K. Gurnon and N. J. Wagner, "Microstructure and rheology relationships for shear thickening colloidal dispersions," Journal of Fluid Mechanics **769**, 242276 (2015).

[40]S. Yamamoto and T. Matsuoka, "Dynamic simulation of fiber suspensions in shear flow," The Journal of Chemical Physics **102**, 2254–2260 (1995), https://doi.org/10.1063/1.468746.

[41]R. C. Ball and J. R. Melrose, "A simulation technique for many spheres in quasi-static motion under frame-invariant pair drag and brownian forces," Physica A: Statistical Mechanics and its Applications **247** (1997), 10.1016/s0378-4371(97)00412-3.

[42]C. Ness and J. Sun, "Flow regime transitions in dense non-brownian suspensions: Rheology, microstructural characterization, and constitutive modeling," Phys. Rev. E **91**, 012201 (2015).

[43]A. J. Banchio and J. F. Brady, "Accelerated stokesian dynamics: Brownian motion," The Journal of Chemical Physics **118**, 10323–10332 (2003), https://doi.org/10.1063/1.1571819.

[44]J. H. Irving and J. G. Kirkwood, "The statistical mechanical theory of transport processes. iv. the equations of hydrodynamics," The Journal of Chemical Physics **18**, 817–829 (1950), https://doi.org/10.1063/1.1747782.

[45]A. Sierou and J. F. Brady, "Rheology and microstructure in concentrated noncolloidal suspensions," Journal of Rheology **46**, 1031–1056 (2002), https://doi.org/10.1122/1.1501925.

[46]E. Bertevas, X. Fan, and R. I. Tanner, "Simulation of the rheological properties of suspensions of oblate spheroidal particles in a newtonian fluid," Rheologica Acta **49**, 53 (2009).

[47]C. D. Cwalina and N. J. Wagner, "Rheology of non-brownian particles suspended in concentrated colloidal dispersions at low particle reynolds number," Journal of Rheology **60**, 47–59 (2016), https://doi.org/10.1122/1.4935445.

[48]A. Vázquez-Quesada, N. J. Wagner, and M. Ellero, "Normal lubrication force between spherical particles immersed in a shear-thickening fluid," Physics of Fluids **30**, 123102 (2018), https://doi.org/10.1063/1.5054067.

[49]R. G. Cox and H. Brenner, "The slow motion of a sphere through a viscous fluid towards a plane surfaceii small gap widths, including inertial effects," Chemical Engineering Science **22**, 1753 – 1777 (1967).

[50]A. J. Goldman, R. G. Cox, and H. Brenner, "Slow viscous motion of a sphere parallel to a plane walli motion through a quiescent fluid," Chemical Engineering Science **22**, 637 – 651 (1967).